AGU PUBLICATIONS

Geophysical Research Letters

RESEARCH LETTER
10.1002/2016GL070470

Key Points:
- Hdeg CCSM4 projects more landfalling winter ARs for Southern California for RCP8.5 scenario due to influences from the subtropical jet
- Landfall changes in ARs affecting UK are projected to be seasonally dependent and influenced primarily by eddy-driven jets
- Causality of future changes to AR landfall location differs dynamically between Pacific and Atlantic ARs

Correspondence to:
C. A. Shields,
shields@ucar.edu

Citation:
Shields, C. A., and J. T. Kiehl (2016), Atmospheric river landfall-latitude changes in future climate simulations, *Geophys. Res. Lett.*, *43*, 8775–8782, doi:10.1002/2016GL070470.

Received 15 JUL 2016
Accepted 8 AUG 2016
Accepted article online 9 AUG 2016
Published online 25 AUG 2016

Atmospheric river landfall-latitude changes in future climate simulations

Christine A. Shields[1] and Jeffrey T. Kiehl[1]

[1]National Center for Atmospheric Research, Boulder, Colorado, USA

Abstract The latitude of landfall for atmospheric rivers (ARs) is examined in the fully coupled half-degree version of the Community Climate System Model, version 4 (CCSM4) for warm future climate simulations. Two regions are examined: U.S. West Coast/North Pacific ARs and United Kingdom/North Atlantic ARs. Changes in AR landfall-latitude reflect changes in the atmospheric steering flow. West Coast U.S. ARs are projected to push equatorward in response to the subtropical jet climate change. UK AR response is dominated by eddy-driven jets and is seasonally dependent. UK simulated AR response is modest in the winter with the largest relative changes occurring in the seasonal transition months. Precipitation associated with ARs is also projected to increase in intensity under global warming. CCSM4 projects a marked shift to higher rainfall rates for Southern California. Small to modest rainfall rates may increase for all UK latitudes, for the Pacific Northwest, and central and northern California.

1. Introduction

Atmospheric rivers (ARs) are long, narrow filamentary extratropical structures that potentially transport or generate large amounts of moisture from the subtropics to the extratropics [*Dettinger*, 2011; *Dettinger et al*., 2011; *Ralph et al*., 2004, 2005, 2011, 2013; *Dacre et al*., 2015]. ARs profoundly impact local hydroclimate by producing major floods [*Lavers and Villarini*, 2013; *Neiman et al*., 2011; *Ralph et al*., 2006] or alleviating drought [*Dettinger*, 2013]. Storm systems such as atmospheric rivers significantly impact today's populated regions, raising the question of how this phenomenon may change under future greenhouse warming. The answer to this question is likely geographically dependent. A number of modeling studies have begun addressing this issue [*Warner et al*., 2015; *Dettinger*, 2011; *Hagos et al*., 2016; *Lavers et al*., 2013; *Shields and Kiehl*, 2016], but with varying conclusions. Most studies point to a world with more ARs, but depending on the AR detection algorithm, the severity of the increase is still an open question. Because ARs track with the steering by atmospheric flow, the jet stream response to global warming must also be evaluated. A variety of model studies generally project a poleward shift in the mean position of the jets with global warming [i.e., *Chang et al*., 2012; *Yin*, 2005; *Mizuta*, 2012; *Lu et al*., 2008]. However, *Payne and Magnusdottir* [2015] show a dependence of North Pacific AR frequency with a broadening of the subtropical jet position using CMIP5 models, and *Barnes and Polvani* [2013] find that geographical area determines the type of jet variability. In the *Barnes and Polvani* [2013] study, Southern Hemisphere and North Atlantic jets are projected to vary in speed or in their "pulsing," whereas the North Pacific jets project stronger variability in the north-south "wobbling," an important distinction that impacts changes to the landfall-latitude of atmospheric rivers in future climate. Other studies have addressed future uncertainties in atmospheric rivers with respect to jet placement by decomposing effects into dynamical and thermodynamical components and find that dynamical changes somewhat counter thermodynamical changes in CMIP5 models for western North America as well as European regions south of the mean jet position [*Gao et al*., 2015, 2016].

Here we employ the moderately high resolution Community Climate System Model, version 4 (CCSM4) to evaluate how changes in atmospheric dynamical flow affect ARs. High horizontal resolution has a number of advantages, the most important being that (1) extreme precipitation is better represented [*Shields et al*., 2016] and (2) higher resolution generally improves AR climatology in the CCSM4 framework compared to ERA-Interim data [*Dee et al*., 2011] by decreasing storm counts (using the high-frequency output methodology employed in this study). *Hagos et al*. [2015] also conducted CAM4 sensitivity experiments testing both resolution and dynamical core and found a general decrease in AR frequency with increasing resolution.

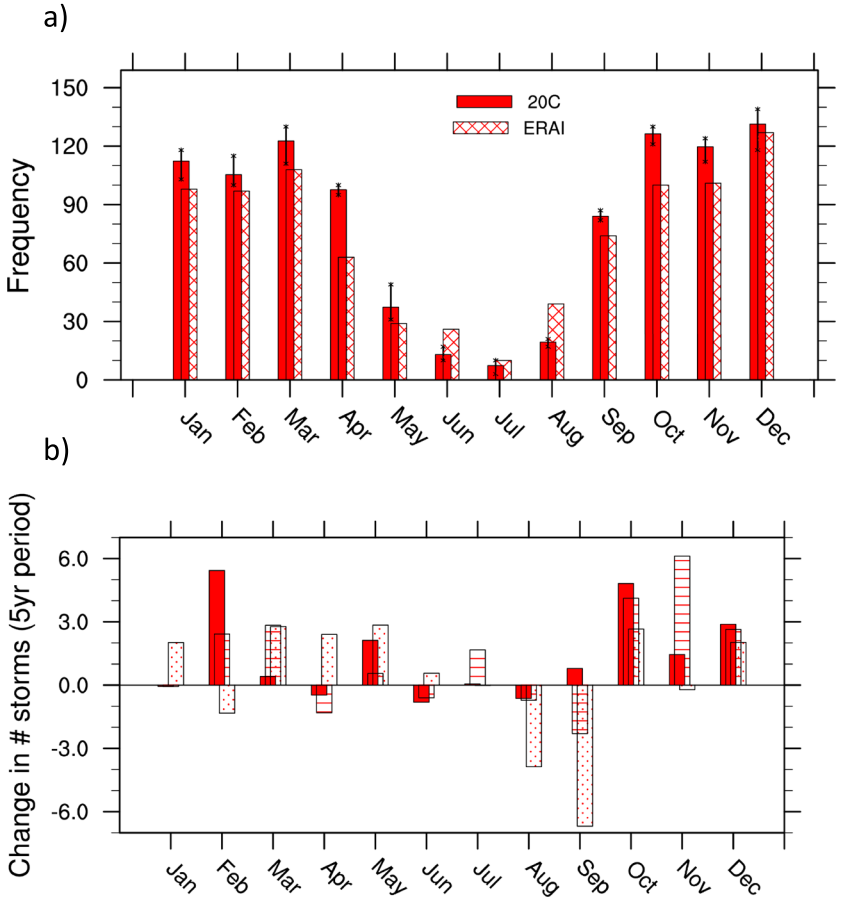

Figure 1. (a) Seasonal cycle of the ensemble mean-simulated UK domain (solid) and ERAI reanalysis (hatched) 1980–2005 and (b) 21st century to 20th century changes to the seasonal cycle for simulated UK ARs for three ensemble members (number of storms/5 year period). Ensemble spread shown in black.

Using AR climatologies, jet analysis, and extreme precipitation statistics, the current study shows that changes in landfall-latitude for North Atlantic ARs are fundamentally different than North Pacific ARs due to differences in jet characteristics.

2. Model Description and Methodology

Results presented were generated using the half-degree version of the fully coupled Community Climate System Model version 4 (CCSM4), which is higher than the standard 1° version and better for representing extreme precipitation [*Shields et al.*, 2016; *Gent et al.*, 2011]. The higher resolution is applied in the atmosphere and land components (Community Atmosphere Model version 4, CAM4, and Community Land Model version 4, CLM4, respectively) with the ocean and sea ice components resolved at nominal 1° (Parallel Ocean Program version 2, POP2, and Community Ice Code, version 4 CICE4, respectively) [*Neale et al.*, 2013; *Lawrence et al.*, 2011; *Smith et al.*, 2010; *Hunke and Lipscomb*, 2008]. The Community Atmosphere Model employs the finite volume dynamical core with 26 layers in the vertical [*Lin*, 2004] with the ocean model resolving 60 layers in the vertical. Climate simulations performed include ensemble suites of historical and RCP8.5 (Representative Concentration Pathway) experiments with five ensemble members for each experiment. However, due to resource constraints, only three ensemble members contain the high-frequency output necessary for AR detection and AR-specific diagnostics. AR statistics and AR-related precipitation use 6-hourly and daily data, respectively. Wind and jet stream diagnostics include all ensemble members and use monthly data.

There are many types of AR detection methods in the literature including, but not limited to, techniques applying integrated water vapor thresholds [*Ralph et al.*, 2004; *Neiman et al.*, 2008], integrated vapor transport

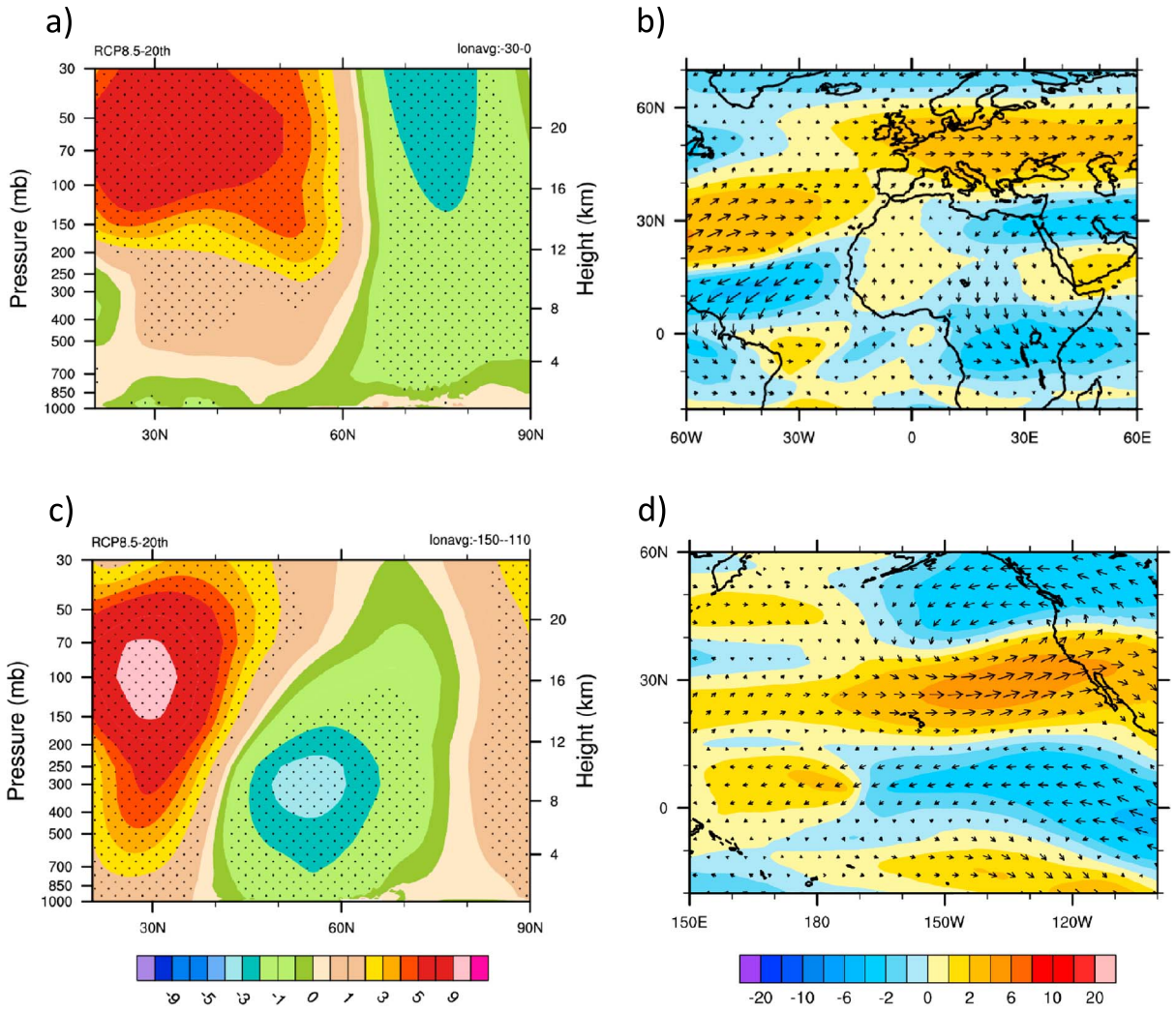

Figure 2. Winter (December-January-February, DJF) climate change (RCP8.5-historical) for (a) zonal wind UK domain (0–30°W); (b) 300 mb total wind magnitude and direction over North Atlantic, Europe, and Africa; (c) same as Figure 2a except for WEST (110–150°W); (d) same as Figure 2b except over North Pacific and western North America. Wind is in m s^{-1} and is plotted with color contours ranging from −9 to +9 in Figures 2a and 2c and ranging from −20 to +20 with a reference vector of 10 m s^{-1} in Figures 2b and 2d. Entire ensemble suite (five members each) is used with statistical significance at 95% stippling for Figures 2a and 2c.

thresholds [*Lavers et al*., 2012; *Guan and Waliser*, 2015; *Warner et al*., 2015], shape identification [*Wick et al*., 2013], and statistical clustering [*Swales et al*., 2016]. Most methodologies incorporate wind and moisture information in their algorithm. This study utilizes an algorithm that includes wind and shape thresholds but, more importantly, applies a moisture threshold that is relative to the background state, such that warm future climate ARs are represented independent of increases due to the Clausius-Clapeyron relationship. *Zhu and Newell* [1998] and *Newman et al*. [2012] describe the empirical formula used here for both historical and RCP8.5 simulations, which computes a unique moisture threshold for each 6 h time period based on mean and maximum values per latitude band. This AR detection methodology applies both total column water and dynamical constraints and was the same as used in *Shields and Kiehl* [2016] for the Pineapple Express (i.e., an atmospheric river extending out of the tropics reaching the west coast of North America). This study, however, evaluates all landfalling U.S. West Coast rivers (32°N–52°N, henceforth called WEST) and all landfalling United Kingdom ARs (49°N–60°N, henceforth called UK). Shape is also considered where thresholds are met across neighboring grid points and maintain a d*y*/d*x* ratio of >2 with a four grid point length minimum. WEST events only include ARs from the southwest (180–270°) and 850 mb wind speeds >10 m s^{-1} [*Dettinger*, 2004, 2011] where UK events include all directions with an easterly component with a higher wind speed threshold of 25 m s^{-1}. Higher wind speeds are used for UK region to eliminate small, less

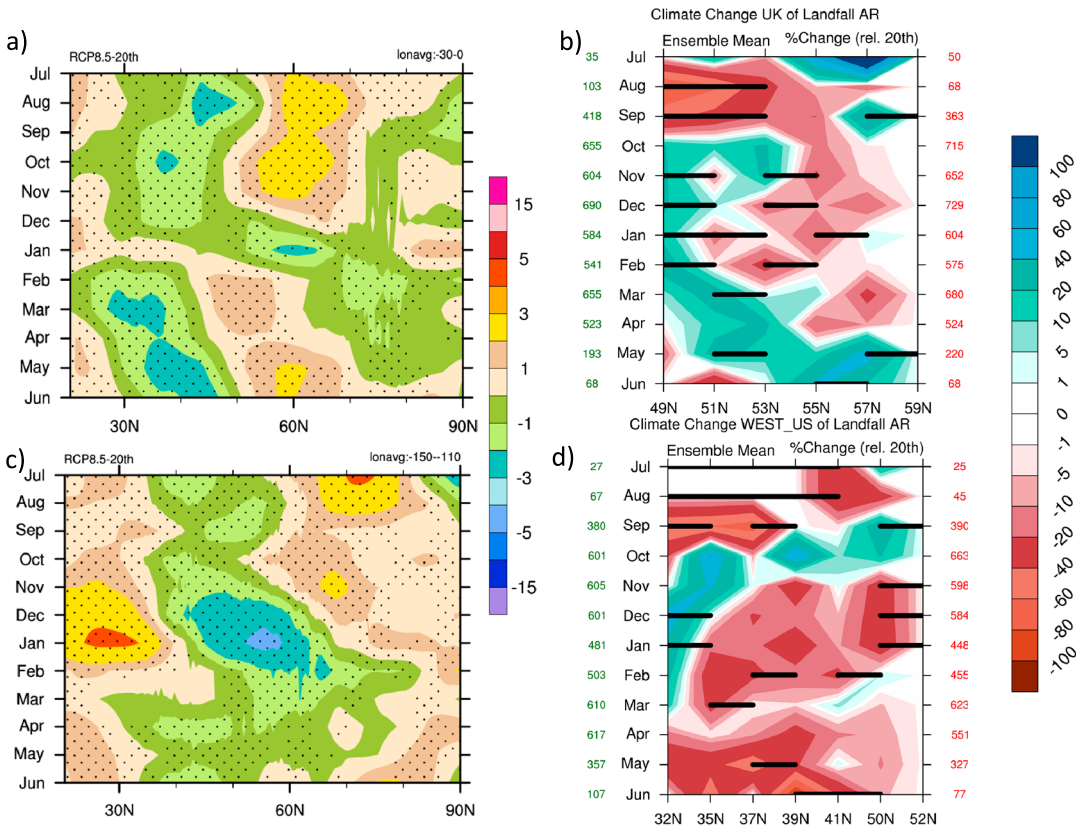

Figure 3. (a) The 850 mb zonal wind climate change (RCP8.5-historical) seasonal cycle versus latitude for UK domain (0–30°W) with 95% significance stippling, (b) AR frequency climate change (RCP8.5-historical/historical) seasonal cycle versus latitude for UK domain, (c) same as Figure 3a except for WEST domain (110–150°W), and (d) same as Figure 3b except for WEST domain. Green (red) numbers in Figures 3b and 3d are ensemble-sum all-latitude storm counts for historical (RCP8.5) for 1960–2005 (2055–2100), and black bars denote significance.

intense localized storm systems that generally have no connection to the subtropics and fall within the top 85th percentile wind magnitudes. Algorithm adjustments are necessary to address geographically specific needs across the different AR regions. Moisture transport over the northeast Pacific Ocean, impacting lower latitudinal areas on the U.S. West Coast, tracks differently than moisture transport over the Northern Hemisphere Atlantic Ocean Basin and thus requires different wind constraints. With a threshold of 25 m s^{-1} over the UK domain, we also find better agreement in the UK AR climatology compared to ERA-Interim reanalysis (Figure 1a) and better agreement with *Lavers and Villarini* [2015] AR UK climatology, which uses a different detection method. Projected UK AR model trends in seasonal climatology under the RCP8.5 scenario are plotted in Figure 1b. There is a high degree of internal variability in these projections with the exception of two cool weather months (October and December). This statistic describes the climatology including all grid points within the domain and does not separate storm counts by latitude. Section 3, however, will decompose this statistic into seasonal climatology by latitude. The Pineapple Express AR climatology, a subset of the WEST climatology, is described in more detail in *Shields and Kiehl* [2016], (Figure 2). We define AR storms as consecutive 6 h periods that meet all criteria and landfall-latitude as the coastal latitudinal location first influenced by an AR system. Biases and uncertainty in the subtropical jet in Community Earth System Model (CESM) modeling framework have been shown to be smaller than the model response to climate change [*Hagos et al.*, 2016]. Hence, here we discuss the model's jet response to climate change and its impact on atmospheric rivers.

3. Results

The subtropical and eddy-driven jets provide steering winds that allow atmospheric rivers to flow into the coastal locations on a given continent. More northern locations, such as UK ARs, are most influenced by

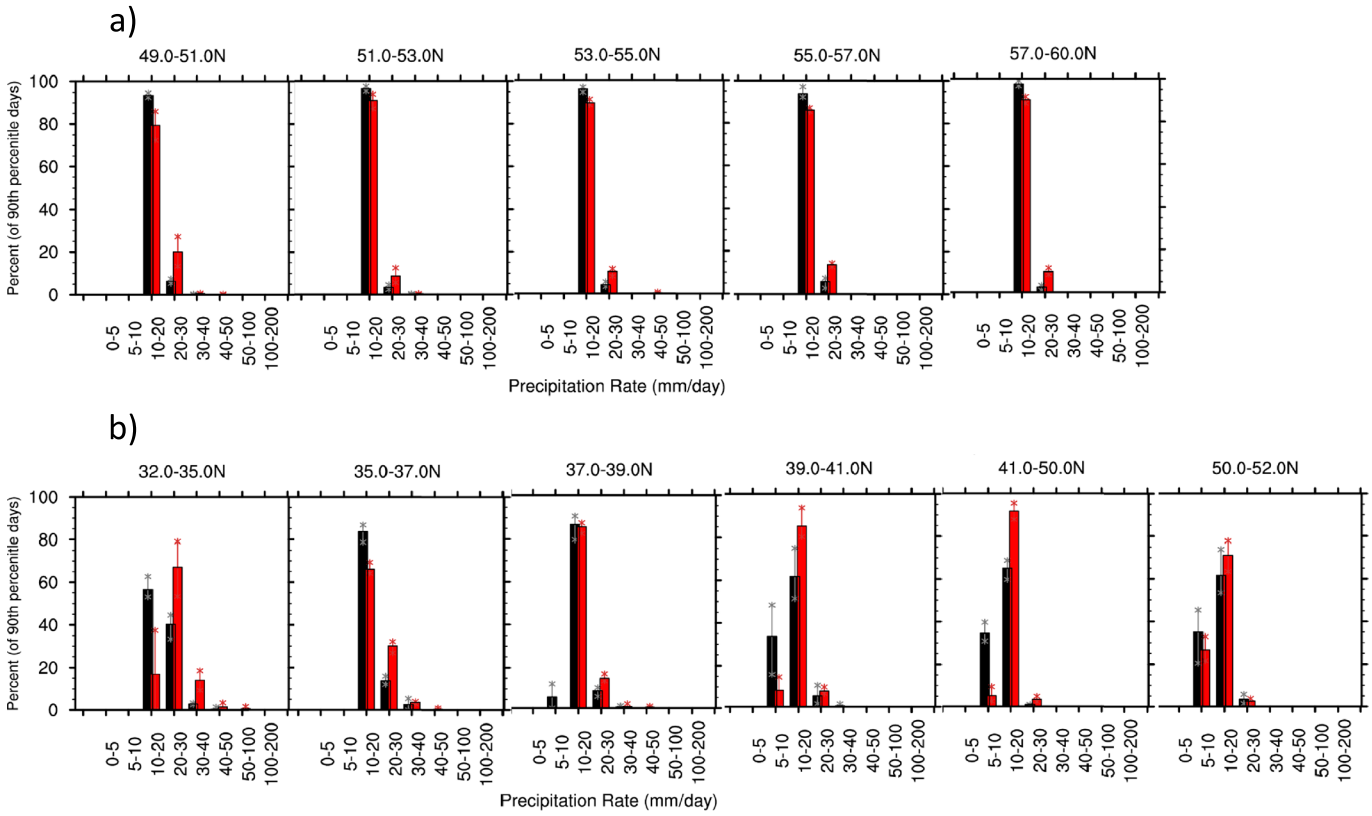

Figure 4. AR precipitation probability density functions for (a) latitude bands spanning WEST domain and (b) latitude bands spanning UK domains. Binning is organized by precipitation rate in mm d^{-1}. Ensemble spread is shown.

eddy-driven jets, whereas the subtropical jet influences the Pineapple Express California locations. As noted in section 1, many papers in the literature project a poleward shift in the jets and storm tracks under global warming scenarios. In CESM, upon closer examination of feedbacks, it has been found that the lack of poleward shift in the winter months for the Northern Hemisphere is due to competing forcing responses from greenhouse gases and sea ice loss [*Deser et al*., 2014, Figures 5 and 6]. In our fully coupled simulations, the more localized domains of WEST and UK experience a different jet response for each of these regions. In Figures 2a and 2c, latitude versus height, winter zonal wind (*U*) climate change is plotted longitudinally averaged between 0 and 30°W for the UK and 110–150°W for the WEST. Wintertime is shown because the strongest storms and highest AR frequency values occur in this season. The UK domain experiences an upper level weakening (strengthening) north (south) of 60°N; however, at lower levels with more typical of AR flow, differences have little statistical significance and exhibit reversal at the surface. The WEST domain, however, shows a clear, significant equatorward strengthening throughout the depth of the atmosphere, particularly enhanced for the subtropical jet region ~30°N. Both of these responses are consistent with a strengthening of the subtropical jet under global warming [*Shepherd and McLandress*, 2011; *Lu et al*., 2007]. Figures 2 and 2d, which show changes in wind direction and magnitude geographically at 300 mb, reinforce this idea. Winds are stronger over the UK and Europe with small changes to the flow itself, which is consistent with *Barnes and Polvani*'s [2013] findings that the North Atlantic jet displays variance in speed, or pulse, more so than north-south variation. (There is no change at the lower levels, not shown.) The subtropical jet over the Atlantic increases in strength ~30°N over open ocean. Its influence is limited to southern European locations such as the Iberian Peninsula. The WEST, however, is more directly influenced by the subtropical jet and projected to increase (decrease) in both flow and magnitude over the southern (northern) part of the domain.

Figure 3 illustrates the connection between AR frequencies to the zonal wind. These Hovmöller plots show the seasonal progression of change in 850 mb *U* (RCP8.5-historical) versus latitude (Figures 3a and 3c) and seasonal AR frequency expressed as mean percent change relative to the twentieth century values

(Figures 3b and 3d). Actual frequency values are given in green and red next to Figures 3b and 3d to indicate total AR counts (all latitude bands and all ensemble members) and to distinguish high percentage values that exist simply because the overall numbers are very small. Some expression of significance describing internal variability (variance among the ensemble members) is also plotted with the horizontal black bars. This is computed by finding the ensemble spread at each month and each latitude band. If the spread does not overlap between historical and RCP8.5 runs, that is, if all RCP8.5 ensemble members are either greater (or less) than the historical ensemble members, significance is assumed. AR frequency is computed for each latitude band (i.e., for the WEST, 32°N–35°N, −37°N, and −39°N) and plotted as contours. For example, the value plotted at 32°N and December describes the 32–35°N latitude band frequency count. Changes in the 850 mb jet roughly approximate changes in AR frequency over the course of the year. For the UK (Figure 3a, 49–60°N), changes in the 850 mb flow are modest in the wintertime. The only detectable poleward shift in AR counts (Figure 3b) occurs in the months of September and May and mirror changes in the eddy-driven jet. For September, this result is entirely latitudinally dependent. Figure 1b hints at a drying tendency; however, once storm counts are broken up into latitude bands, only southern (northern) UK locations show a reduction (enhancement) in ARs. Modest increases in wintertime AR UK counts (Figure 3b) are found in the southern part of the domain and do not correspond to the strongest jet changes. For the WEST, an obvious and significant winter equatorward shift in ARs toward the more southern latitude bands occurs in response to the subtropical jet response. There is also a remarkable reduction in AR frequency across more northern latitude bands for most of the year. October is the only month projected to experience an increase in AR frequency; however, this result is not robust due to the variability across ensemble members.

To test the robustness of this response, we plot AR 90th percentile precipitation probability density functions in Figure 4. AR precipitation was calculated by matching storm events with precipitation records for those exact periods, over the specified latitude bands, for both WEST and UK domains. UK locations display a modest shift into higher rainfall rate bins across all latitude bands in the RCP8.5 scenario simulations. This is consistent with findings in the literature that project an increase in more intense rainfall rates in a warmer world [*Pendergrass and Hartmann*, 2014; *Kharin et al*., 2013; *Shields et al*., 2016]. However, this modest increase does not change the shape of the UK distribution across rainfall rate bins. The majority of the precipitation still falls within the 10–20 mm/d range. For WEST locations, the precipitation associated with ARs is not only more intense, but the shape of the distribution shifts such that for the 32–25°N latitude band, the majority of precipitation falls within the 20–30 mm/d range. As precipitation progresses northward, however, the distributions appear more similar with only modest increases in the higher bins and are more similar to the UK result. The shift in the 32–35°N latitude band is consistent with the AR frequency and zonal wind plots and confirms a shift in AR frequency equatorward along the U.S. West Coast.

4. Conclusions

We show an equatorward shift in the WEST landfall-latitude cool season climatology under a warming world, which is dominated by the subtropical jet response. WEST ARs increase in the 32°N–35°N latitude bands, as do intense precipitation. These results are consistent with *Payne and Magnusdottir* [2015] who, using an independent AR detection algorithm, have also shown an equatorward response to climate change in U.S. West Coast ARs. With the possible exception of October, all other WEST latitudes for most months are projected to experience a decrease in AR storms. The UK AR response, dominated by eddy-driven jets, is more ambiguous and depends on both the time of year and latitude of landfall. The weak response of the eddy-driven jet over the North Atlantic explains the modest change in AR frequencies over winter. Seasonal transition months, such as September and May, indicate a potential increase in ARs, but changes are likely latitudinally dependent and track with the steering flow. Rainfall rates associated with UK ARs may increase slightly but with no latitudinal distinction.

Acknowledgments
NCAR and CESM are sponsored by the National Science Foundation (NSF). We would like to thank Adrianne Middleton, Frederic Castruccio, and Joanie Kleypas for their contributions in helping complete the half-degree CCSM4 simulation suite. Data from all simulations are available through the Earth System Grid. Please direct Hdeg data requests to shields@ucar.edu. Portions of this study were supported by the Regional and Global Climate Modeling Program (RGCM) of the U.S. Department of Energy's Office of Biological and Environmental Research (BER) Cooperative Agreement DE-FC02-97ER62402 and the National Science Foundation. Computing resources (ark:/85065/d7wd3xhc) were provided by the Climate Simulation Laboratory at NCAR's Computational and Information Systems Laboratory, sponsored by the National Science Foundation and other agencies. An award of computer time was also provided by the Innovative and Novel Computational Impact on Theory and Experiment (INCITE) program and used the resources of Oak Ridge Leadership Computing Facility located in the Oak Ridge National Laboratory, which is supported by the Office of Science of the Department of Energy under contract DE-AC05-00OR22725. We also thank two anonymous reviewers for their helpful comments.

References

Barnes, E. A., and L. Polvani (2013), Response of the midlatitude jets, and of their variability, to increased greenhouse gases in the CMIP5 models, *J. Clim.*, *26*(18), 7117–7135.

Chang, E. K. M., Y. Guo, and X. Xia (2012), CMIP5 multimodel ensemble projection of storm track change under global warming, *J. Geophys. Res.*, *117*, D23118, doi:10.1029/2012JD018578.

Dacre, H. F., P. A. Clark, O. Martinez-Alvarado, M. A. Stringer, and D. A. Lavers (2015), How do atmospheric rivers form?, *Bull. Am. Meteorol. Soc.*, *96*(8), 1243–1255.

Dee, D. P., et al. (2011), The ERA-Interim reanalysis: Configuration and performance of the data assimilation system, *Q. J. R. Meteorol. Soc.*, *137*(656), 553–597.
Deser, C., R. A. Tomas, and L. Sun (2014), The role of ocean–atmosphere coupling in the zonal-mean atmospheric response to Arctic sea ice loss, *J. Clim.*, *28*(6), 2168–2186.
Dettinger, M. (2004), Fifty-two years of Pineapple-Express storms across the west coast of North America. California Energy Commission PIER Energy-Related Environmental Research Report CEC-500-2005-004, Sacramento, California, 15 pp.
Dettinger, M. D. (2011), Climate change, atmospheric rivers, and floods in California—A multimodel analysis of storm frequency and magnitude changes, *J. Am. Water Resour. Assoc.*, *47*(3), 514–523.
Dettinger, M. D. (2013), Atmospheric rivers as drought busters on the U.S. West Coast, *J. Hydrol.*, *14*(6), 1721–1732.
Dettinger, M. D., F. M. Ralph, T. Das, P. J. Neiman, and D. Cayan (2011), Atmospheric rivers, floods, and the water resources of California, *Water*, *3*, 455–478.
Gao, Y., J. Lu, L. R. Leung, Q. Yang, S. Hagos, and Y. Qian (2015), Dynamical and thermodynamical modulations on future changes of landfalling atmospheric rivers over western North America, *Geophys. Res. Lett.*, *42*, 7179–7186, doi:10.1002/2015GL065435.
Gao, Y., J. Lu, and L. R. Leung (2016), Uncertainties in projecting future changes in atmospheric rivers and their impacts on heavy precipitation over Europe, *J. Clim.*, doi:10.1175/JCLI-D-16-0088.1.
Gent, P. R., et al. (2011), The Community Climate System Model version 4, *J. Clim.*, *24*, 4973–4991.
Guan, B., and D. E. Waliser (2015), Detection of atmospheric rivers: Evaluation and application of an algorithm for global studies, *J. Geophys. Res. Atmos.*, *120*, 12,514–12,535, doi:10.1002/2015JD024257.
Hagos, S. M., L. Ruby Leung, Q. Yang, C. Zhao, and J. Lu (2015), Resolution and dynamical core dependence of atmospheric river frequency in global model simulations, *J. Clim.*, *28*(7), 2764–2776.
Hagos, S. M., L. R. Leung, J.-H. Yoon, J. Lu, and Y. Gao (2016), A projection of changes in landfalling atmospheric river frequency and extreme precipitation over western North America from the Large Ensemble CESM simulations, *Geophys. Res. Lett.*, *43*, 1357–1363, doi:10.1002/2015GL067392.
Hunke, E. C., and W. H. Lipscomb (2008), CICE: The Los Alamos sea ice model user's manual, version 4. Los Alamos National Laboratory Tech. Rep. LA-CC-06-012, 76pp.
Kharin, V. V., F. W. Zwiers, X. Zhang, and M. Wehner (2013), Changes in temperature and precipitation extremes in the CMIP5 ensemble, *Clim. Chang*, *119*, 345–57.
Lavers, D. A., and G. Villarini (2013), The nexus between atmospheric rivers and extreme precipitation across Europe, *Geophys. Res. Lett.*, *40*, 3259–3264, doi:10.1002/grl.50636.
Lavers, D. A., and G. Villarini (2015), The contribution of atmospheric rivers to precipitation in Europe and the United States, *J. Hydrol.*, *522*, 382–390, doi:10.1016/j.jhydrol.2014.12.010.
Lavers, D. A., G. Villarini, R. P. Allan, E. F. Wood, and A. J. Wade (2012), The detection of atmospheric rivers in atmospheric reanalyses and their links to British winter floods and the large-scale climatic circulation, *J. Geophys. Res.*, *117*, D20106, doi:10.1029/2012JD018027.
Lavers, D. A., R. P. Allan, G. Villarini, B. Lloyd-Hughes, D. J. Brayshaw, and A. J. Wade (2013), Future changes in atmospheric rivers and their implications for winter flooding in Britain, *Environ. Res. Lett.*, *8*, 034,010, doi:10.1088/1748-9326/8/3/034010.
Lawrence, D. M., et al. (2011), Parameterization improvements and functional and structural advances in version 4 of the Community Land Model, *J. Adv. Model. Earth Syst.*, *3*, M03001, doi:10.1029/2011MS000045.
Lin, S. J. (2004), A "vertically Lagrangian" finite-volume dynamical core for global models, *Mon. Weather Rev.*, *132*, 2293–2307.
Lu, J., G. A. Vecchi, and T. Reichler (2007), Expansion of the Hadley cell under global warming, *Geophys. Res. Lett.*, *34*, L06805, do:10.1029/2006GL028443.
Lu, J., G. Chen, M. Dargan, and N. S. M. W. Frierson (2008), Response of the zonal mean atmospheric circulation to El Niño versus global warming, *J. Clim.*, *21*(22), 5835–5851.
Mizuta, R. (2012), Intensification of extratropical cyclones associated with the polar jet change in the CMIP5 global warming projections, *Geophys. Res. Lett.*, *39*, L19707, doi:10.1029/2012GL053032.
Neale, R. B., J. Richter, S. Park, P. H. Lauritzen, S. J. Vavrus, P. J. Rasch, and M. Zhang (2013), The mean climate of the Community Atmosphere Model (CAM4) in forced SST and fully coupled experiments, *J. Clim.*, *26*, 5150–5168, doi:10.1175/JCLI-D-12-00236.1.
Neiman, P. J., F. M. Ralph, G. A. Wick, J. D. Lundquist, and M. D. Dettinger (2008), Meteorological characteristics and overland precipitation impacts of atmospheric rivers affecting the West Coast of North America based on eight years of SSM/I satellite observations, *J. Hydrometeol.*, *9*, 22–47.
Neiman, P. J., L. J. Schick, F. M. Ralph, M. Hughes, and G. A. Wick (2011), Flooding in Western Washington: The connection to atmospheric rivers, *J. Hydrol.*, *12*(6), 1337–1358.
Newman, M., G. N. Kiladis, K. M. Weickmann, F. M. Ralph, and P. D. Sardeshmukh (2012), Relative contributions of synoptic and low-frequency eddies to time-mean atmospheric moisture transport, including the role of atmospheric rivers, *J. Clim.*, *25*, 7341–7361.
Payne, A. E., and G. Magnusdottir (2015), An evaluation of atmospheric rivers over the North Pacific in CMIP5 and their response to warming under RCP 8.5, *J. Geophys. Res. Atmos.*, *120*, 11,173–11,190, doi:10.1002/2015JD023586.
Pendergrass, A. G., and D. L. Hartmann (2014), Changes in the distribution of rain frequency and intensity in response to global warming, *J. Clim.*, *27*(22), 8372–8383.
Ralph, F. M., P. J. Neiman, and G. A. Wick (2004), Satellite and CALJET aircraft observations of atmospheric rivers over the eastern North-Pacific Ocean during the El Niño winter of 1997/98, *Mon. Weather Rev.*, *132*, 1721–1745.
Ralph, F. M., P. J. Neiman, and R. Rotunno (2005), Dropsonde observations in low-level jets over the northeastern Pacific Ocean from CALJET-1998 and PACJET-2001: Mean vertical-profile and atmospheric-river characteristics, *Mon. Weather Rev.*, doi:10.1175/MWR2896.1.
Ralph, F. M., P. J. Neiman, G. A. Wick, S. I. Gutman, M. D. Dettinger, D. R. Cayan, and A. B. White, (2006), Flooding on California's Russian River: Role of atmospheric rivers, *Geophys. Res. Lett.*, *33*, L13801, doi:10.1029/2006GL026689.
Ralph, F. M., P. J. Neiman, G. N. Kiladis, K. Weickmann, and D. W. Reynolds (2011), A multiscale observational case study of a Pacific atmospheric river exhibiting tropical extratropical connections and a mesoscale frontal wave, *Mon. Weather Rev.*, doi:10.1175/2010MWR3596.1.
Ralph, F. M., T. Coleman, P. J. Neiman, J. Zamora, and M. D. Dettinger (2013), Observed impacts of duration and seasonality of atmospheric-river landfalls on soil moisture and runoff in coastal Northern California, *J. Hydrol. Meteorology*, doi:10.1175/JHM-D-12-076.1.
Shepherd, T. G., and C. McLandress (2011), A robust mechanism for strengthening of the Brewer-Dobson circulation in response to climate change: Critical-layer control of subtropical wave breaking, *J. Atmos. Sci.*, *68*(4), 784–797.
Shields, C. A., and J. T. Kiehl (2016), Simulating the Pineapple Express in the half degree Community Climate System Model, CCSM4, *Geophys. Res. Lett.*, *43*, doi:10.1002/2016GL069476.

Shields, C. A., J. T. Kiehl, and G. A. Meehl (2016), Future changes in regional precipitation simulated by a half-degree coupled climate model: Sensitivity to horizontal resolution, *JAMES*, doi:10.1002/2015MS000584.

Smith, R. D., et al. (2010), The Parallel Ocean Program (POP) reference manual, Tech. Rep. LAUR-10-01853, Los Alamos Natl. Lab., Los Alamos. [Available http://www.cesm.ucar.edu/models/cesm1.0/pop2/doc/sci/POPRefManual.pdf.]

Swales, D., M. Alexander, and M. Hughes (2016), Examining moisture pathways and extreme precipitation in the U.S. Intermountain West using self-organizing maps, *Geophys. Res. Lett.*, *43*, 1727–1735, doi:10.1002/2015GL067478.

Warner, M. D., C. F. Mass, and E. P. Salathe (2015), Changes in winter atmospheric rivers along the North American west coast in CMIP5 climate models, *J. Hydrol. Meteorol.*, doi:10.1175/JHM-D-14-0080.1.

Wick, G. A., P. J. Neiman, and F. M. Ralph (2013), Description and validation of an automated objective technique for identification and characterization of the integrated water vapor signature of atmospheric rivers, *Trans. On Geoscience Rem. Sens.*, *51*, 4.

Yin, J. H. (2005), A consistent poleward shift of the storm tracks in simulations of 21st century climate, *Geophys. Res. Lett.*, *32*, L18701, doi:10.1029/2005GL023684.

Zhu, Y., and R. E. Newell (1998), A proposed algorithm for moisture fluxes from atmospheric rivers, *Mon. Weather Rev.*, *126*(3), 725–735, doi:10.1175/1520-0493(1998)126<0725:APAFMF>2.0.CO;2.